Journal of Power Sources 182 (2008) 489–495

Contents lists available at ScienceDirect

Journal of Power Sources

journal homepage: www.elsevier.com/locate/jpowsour

Application of nitrogen-rich amino acids to active site generation in oxygen reduction catalyst

Jun Maruyama[a,*], Nobutaka Fukui[b], Masayuki Kawaguchi[b], Ikuo Abe[a]

[a] Environmental Technology Department, Osaka Municipal Technical Research Institute, 1-6-50, Morinomiya, Joto-ku, Osaka 536-8553, Japan
[b] Graduate School of Engineering, Osaka Electro-Communication University, 18-8, Hatsu-cho, Neyagawa, Osaka 572-8530, Japan

ARTICLE INFO

Article history:
Received 13 March 2008
Accepted 10 April 2008
Available online 25 April 2008

Keywords:
Polymer electrolyte fuel cell
Noble-metal-free catalyst
Oxygen reduction
Amino acid

ABSTRACT

Noble-metal-free catalysts are demanded for widespread use of polymer electrolyte fuel cells (PEFCs) and the activity enhancement is required for practical use in the PEFC. We showed previously that a heat treatment of a mixture of iron lactate, glucose, and glycine generated a carbon material with Fe–N_4 moiety as the active site for cathodic oxygen reduction; although the activity was still lower than conventional Pt-based PEFC cathode catalysts. In this study, the carbon-based noble-metal-free PEFC cathode catalyst was formed using amino acids containing more than one nitrogen atom in the molecule as the nitrogen source in order to obtain fundamental information on the efficient formation of the active site and the activity enhancement. We found that the oxygen reduction currents measured using rotating disk electrodes with the catalyst fixed on the surface were dependent on the amino acid molecular structure. The activity of the catalyst increased with an increase in the number of nitrogen atoms contained in the amino acid. The activity increase was attributed to the improved efficiency of the active site generation, based on the Fe contents, X-ray photoelectron spectra, and the extended X-ray adsorption fine structures at the Fe K-edge of the carbon material.

1. Introduction

Catalysts free from noble metals have recently attracted much attention, especially in the research and development of polymer electrolyte fuel cells (PEFCs). The high-energy conversion efficiency and minimized environment pollution, which are promising properties of the PEFC as a new electricity generation system, have been demonstrated using platinum-based catalysts consisting of dispersed platinum or platinum alloys and carbon support in the electrodes. Solving the problems of resource limitations and the possible cost inflation which are associated with such Pt-based catalysts by developing the noble-metal-free catalysts would begin the PEFC widespread use leading to the global environment improvement [1–5]. Especially, the PEFC cathode are demanded due to the slow reaction rate of O_2 reduction, which requires a sufficient amount of Pt [6]. However, the noble-metal-free catalysts with sufficient activity and reliability for the PEFC electrode reactions to substitute the Pt-based catalysts have not been developed so far [7].

Among various types of noble-metal-free fuel cell cathode catalysts [8–11], carbon materials with Fe ion coordinated by nitrogen atoms (Fe–N_x moiety) embedded on the surface as the active site have been most extensively studied and are one of the promising candidates for the active and reliable catalyst [12–41]. Several methods have been reported to produce the carbon materials with the Fe–N_x active site: (a) heat treatment of a complex usually adsorbed on carbon materials, in which Fe is coordinated by nitrogen atoms in the ligands, such as porphyrins [12–29], phthalocyanine [30,31], phenanthroline [32], cynanide [33]; (b) heat treatment of a mixture of Fe salts and a nitrogen-containing polymer such as polypyrrole and polyacrylonitrile with or without carbon black [34–38]; (c) heat treatment of the Fe salts supported on carbon materials in NH_3 or CH_3CN gases [25,28,39,40]; (d) heat treatment of the Fe salts loaded on carbon materials which are enriched with nitrogen on the surface or formed by carbonization in the NH_3 gas [25,26,41]. We recently formed the noble-metal-free cathode catalysts by carbonizing catalase and hemoglobin [42–44]. Especially, the abundance and inexpensiveness of hemoglobin are opposite to those of Pt. Hemoglobin could be abundantly obtained (about 2 million tons per year), especially from the meat industry that produces more than 200 million tons of meat per year around the world and discarding blood containing hemoglobin as waste. The active site for the O_2 reduction in these catalysts was assumed to be Fe coordinated by four pyrrolic nitrogen atoms (Fe–N_4 moiety) embedded on the surface of the carbon material, which was derived from protoheme in catalase and hemoglobin.

* Corresponding author. Tel.: +81 6 6963 8043; fax: +81 6 6963 8049.
E-mail address: maruyama@omtri.city.osaka.jp (J. Maruyama).

0378-7753/$ – see front matter © 2008 Elsevier B.V. All rights reserved.
doi:10.1016/j.jpowsour.2008.04.040

This assumption was based on the Mössbauer spectrum of the carbonized catalase [42] and other previous studies reporting that the porphyrin-like structures were retained in the carboneous compounds after the pyrolysis of their precursor which contained metal porphyrins, based on an analysis by X-ray photoelectron spectroscopy [17], X-ray adsorption near-edge structure spectroscopy [45], and Mössbauer spectroscopy [46].

We also developed another method for the formation of the cathode catalyst with the Fe–N_4 moiety [47]. Being prompted by the facts that porphyrin macrocycles of heme are biosynthesized from glycine and that Fe^{2+} is introduced into the center of the porphyrins to form heme, we used Fe(II) lactate and glycine as starting materials for the formation of the Fe–N_x type catalysts. Glucose, the most familiar monosaccharide, was added for obtaining carbon materials, since amino acids alone decompose below 350 °C to result in the failure of carbonization. We found that heat treatments of the mixture of these compounds generated a heme-like active site in the obtained carbon material. The Mössbauer spectrum of the carbon material was similar to that of carbonized catalase, in which the Fe–N_4 moiety was derived from the heme. The X-ray photoelectron spectrum (XPS) of N 1s of the carbon material indicated that the nitrogen atoms of the Fe–N_4 moiety were attributed to the pyrrole-like nitrogen, which was in agreement with the center of the heme structure. The result thus indicated that the nitrogen atoms from glycine and Fe were spontaneously organized into the heme-like structure during pyrolysis and that the formation of the Fe–N_4 moiety in the carbon material was possible by heat treatment of heme and also directly by pyrolysis of the starting molecule for its biosynthesis. We determined that the carbon material possessed activity for cathodic O_2 reduction and the ability to function as a cathode catalyst for the PEFC, which implied the finding of another route for the formation of the Fe–N_x type catalysts using simple, biologically familiar and abundant molecules as starting materials. Although the activity was comparable to the Fe–N_x type catalysts that have been reported before, it was still lower than that of the conventional Pt-based catalysts. However, we found that an increase in the glycine content in the starting mixture improved the activity, indicating that the amount of the Fe–N_x active site was increased by an increase in the amount of the nitrogen source.

There are several amino acids containing more than one nitrogen atom in each molecule. In this study, we investigated the noble-metal-free catalysts formed using such nitrogen-rich amino acids as the nitrogen source for the Fe–N_x active site based on the flexibility of this catalyst formation method with respect to the starting material [48], in order to obtain fundamental information on its efficient formation and the activity enhancement. Among the 20 amino acids constituting proteins, six amino acids contain more than one nitrogen atom in each molecule and were used in this study. They were tryptophan (W), asparagine (N), glutamine (Q), lysine (K), histidine (H), and arginine (R). Their molecular structures, as well as that of glycine (G) for comparison, are shown in Fig. 1.

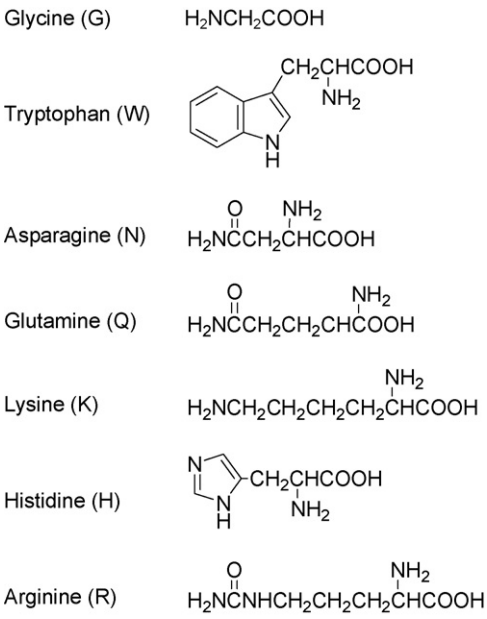

Fig. 1. Molecular structures of amino acids containing more than one nitrogen atom among the 20 amino acids constituting proteins. The molecular structure of glycine, which is the simplest amino acid, is also shown for comparison.

2. Experimental

2.1. Materials

The amino acids, glucose, and iron(II) lactate trihydrate were purchased from Nacalai Tesque and used as received. High-purity water was obtained by circulating ion-exchanged water through an Easypure water-purification system (Barnstead, D7403). Perchloric acid (70%, Tama Chemicals, ultra pure analytical reagent) and sulfuric acid (98%, Tama Chemicals, ultra pure analytical reagent) were diluted with high-purity water to prepare 0.1 mol dm^{-3} $HClO_4$ and 0.5 mol dm^{-3} H_2SO_4, respectively. Solutions of Nafion as a perfluorosulfonate ion-exchange resin (equivalent weight (molar mass/mol of ion-exchange site) = 1100, 5 wt% dissolved in a mixture of lower aliphatic alcohols and 15–20% water) were purchased from Aldrich.

2.2. Formation of the carbon material with an Fe–N_x active site

The amino acid, glucose, and iron(II) lactate trihydrate were mixed and ground with a mortar until all of the powder passed a 100-mesh sieve (aperture, 150 μm). The molar ratio of the amino acid to glucose was set at 1 and the Fe content in the mixture was 1 wt%. The Fe content was set to add a sufficient amount of Fe in the mixture, based on the study by Wang et al. reporting that the activity of the Fe–N_x type catalyst was dependent on the Fe loading and reached the maximum at 0.16–2 wt% [41]. The mixture was heated at 150 °C in air for 24 h for dehydration of glucose, which is often carried out before the carbonization of glucose. After grinding this dehydrated mixture similarly, the powder was heated in 100 cm^3 min^{-1} of flowing Ar at 1000 °C for 2 h after raising the temperature at 5 °C min^{-1}. The sample was ground again until all of the powder passed through a 330-mesh sieve (aperture, 45 μm) and a treatment with an acid solution was carried out to remove soluble Fe species. The treatment was performed in 0.5 mol dm^{-3} H_2SO_4 at a boiling temperature for 1 h, followed by filtering, washing with high-purity water, and drying in vacuum at room temperature. For convenience, the sample produced using X (X = W, N, K, Q, H, R) is hereafter called GXI. The sample using glycine was produced similarly for comparison and is hereafter called GGI.

2.3. Characterization of the carbon materials

The Fe contents in the carbon materials were measured by inductively coupled plasma atomic emission spectrophotometry (ICP-AES) using an ICPS-8100 system (Shimadzu) after combustion of the carbon matrix and dissolution of the residue by 0.5 mol dm^{-3} H_2SO_4 at a boiling temperature. The adsorption isotherm of N_2 onto

Table 1
Yields, Fe contents, and specific surface area (S) of GXI (X = G, W, N, Q, K, H, R)

	Yield (%)			Fe content (wt%)	S ($m^2\,g^{-1}$)
	Heat treatment at 150 °C	Heat treatment at 1000 °C	Total		
GGI	58.3	15.4	9.0	0.14	389
GWI	77.9	8.8	6.8	0.15	318
GNI	70.2	18.5	13.0	0.27	211
GQI	66.8	25.9	17.3	0.40	196
GKI	58.4	20.4	11.9	0.28	175
GHI	74.8	15.8	11.8	0.32	185
GRI	69.8	23.4	16.3	0.37	221

the carbon material was measured using an automatic N_2 adsorption apparatus (Belsorp 28, Nihon Bell) at −196 °C. The specific surface area was determined by the Brunauer–Emmet–Teller (BET) plot of the isotherm. The X-ray diffraction (XRD) was performed with an automated RINT 2500 X-ray diffractometer (Rigaku) using Cu Kα radiation. The data acquisition was carried out in the $\theta/2\theta$ step scanning mode at a speed of 1° min^{-1} with a step size of 0.02° (2θ). The X-ray photoelectron spectroscopy (XPS) was carried out using a PHI ESCA 5700 system (Physical Electronics) with Al Kα radiation (1486.6 eV), in which the finely ground carbonized material was fixed on an Al adhesive tape. The measurements of the extended X-ray absorption fine structures (EXAFS) of the catalyst powder were performed in the transmission mode in air at room temperature using synchrotron radiation at the beam lines of BL19B2 of the SPring8 in the Japan Synchrotron Radiation Research Institute. Fourier transformation was performed on a k^3-weighted EXAFS spectrum using a REX2000 program (Rigaku) to calculate the pseudo-radial distribution function (RDF).

2.4. Catalyst layer formation

The electrochemical characteristics of the carbon material were investigated by fixing it on the surface of a rotating glassy carbon disk electrode (GC RDE) as a catalyst layer and immersing it in 0.1 mol dm^{-3} $HClO_4$ [49–51]. An aliquot of 50 mg of the carbon material and 5 mg of carbon black (Vulcan XC-72R, Cabot) as the electron-conductive agent were added to 1.0 cm^3 of a Nafion solution which was prepared by diluting 0.5 cm^3 of the 5 wt% Nafion solution with high-purity water. The mixture was ultrasonically dispersed to produce a catalyst paste. A GC RDE (BAS), which consisted of a GC rod sealed in a Kel-F holder, was polished with a 2000 grit emery paper (Sumitomo 3 M) and then ultrasonically cleaned in high-purity water for use as a support for the catalyst layer. The geometric surface area of the electrode was 0.071 cm^2 (diameter, 3 mm). A 1 mm^3 volume of the paste was pipetted onto the GC surface, and to shield it from the irregular air stream generated by a ventilator, the electrode was immediately placed under a glass cover until the layer was formed. This operation was repeated once again to load 100 μg of the carbon material on the GC surface. After removal of the glass cover, the layer was further dried overnight at room temperature.

2.5. Electrochemical measurements

An electrochemical analyzer (100B/W, BAS) and an RDE glass cell were used for cyclic voltammetry and measurements of the current–potential relationships. The glass cell was cleaned by soaking in a 1:1 mixture of concentrated HNO_3 and H_2SO_4, followed by a thorough rinsing with high-purity water, and finally steam cleaning [52]. The counter electrode was a Pt wire, and the reference electrode was a reversible hydrogen electrode (RHE). All potentials were referred to the RHE. Cyclic voltammograms for the catalyst layers were recorded in Ar-saturated 0.1 mol dm^{-3} $HClO_4$ at 25 °C. The potential was scanned between 0.05 and 1.3 V at a scan rate of 50 mV s^{-1}. Before recording, the potential was repeatedly scanned between 0.05 and 1.4 V to remove any residual impurities. The current–potential relationships were obtained in O_2-saturated 0.1 mol dm^{-3} $HClO_4$ at 25 °C at various rotation speeds. The scan rate of the potential was fixed at 10 mV s^{-1}. Prior to measurement, the electrode was repeatedly and alternately polarized at 0.05 and 1.3 V [53]. The potential was finally stepped to 1.2 V and then swept in the negative direction to obtain the current–potential relationship. The background current was similarly measured in an Ar atmosphere without rotation.

3. Results and discussion

3.1. Formation of carbon materials

The heat treatment of the mixture of the amino acid, glucose, and Fe(II) lactate trihydrate at 150 °C in air for 24 h produced the precursor and the heat treatment of the precursor at 1000 °C in flowing Ar for 2 h produced the carbon material. The yields of the precursors and those of the carbon materials are summarized in Table 1. The total yield was calculated by multiplying the yield of the precursor by that of the corresponding carbon material from the precursor. These yields were varied with the kind of amino acid; however, a clear relationship between the yields and the kind of the amino acid was absent. The structural regularity of the carbon matrix was also nearly independent of the kind of amino acid. Fig. 2 shows the XRD spectra of the carbon materials. These spectra are typical of amorphous carbon, such as carbon black and activated carbon. The sharp (0 0 2) diffraction peak at 26°, the (1 0) peak at 43°, and the very weak (0 0 4) peak at 53° were observed for all the carbon materials. The absence of ($h\,k\,l$) diffraction peaks except the (0 0 l) peaks was attributed to a structure consisting of randomly layered graphene sheets (turbostratic structure). The intensities of these peaks slightly increased at GKI and decreased at GWI compared to GGI. The small peaks observed for GRI at 33° and 35° were attributed to α- and γ-Fe_2O_3, respectively, probably included in the carbon matrix and retained after the acid treatment of the carbon material.

In contrast, the Fe content tended to increase with an increase in the number of nitrogen atoms contained in the amino acid. In addition, the specific surface areas of the carbon materials formed using the nitrogen-rich amino acids were smaller than that of GGI. These tendencies were also observed for the carbon materials formed using the mixture of glycine, glucose, and Fe lactate, in which the molar ratio of glycine to glucose increased from 1 (the value used for the GGI formation) to 2–4, as was reported previously [47]. The carbon material formed using the mixture in which the glycine/glucose molar ratio was (m = 2–4) is hereafter called GmGI. The pore sizes in the carbon material formed using the nitrogen-rich amino acids

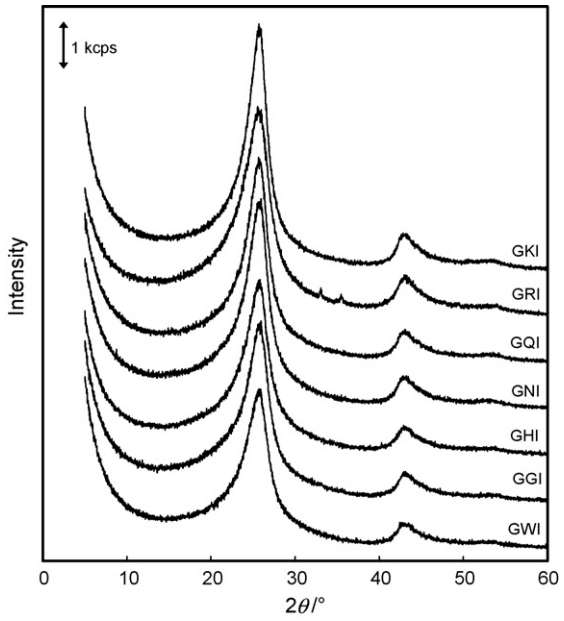

Fig. 2. X-ray diffraction spectra of GGI, GWI, GNI, GQI, GKI, GHI, and GRI. Cu Kα radiation was used. Each spectrum is shifted by 1 kcps for easier comparison.

were also smaller than that in GGI except GWI. The pore-size distributions of the carbon materials are shown in Fig. 3. Those for GQI and GKI were almost the same as that for GHI. The exceptionally large pore size in GWI might be associated with the molecular structure of W, which only contains two aromatic rings, although the detailed mechanism for the pore enlargement was unclear at present.

3.2. Cyclic voltammetry

The surface of the carbon material in contact with the electrolyte becomes electrochemically active where electrochemical reactions occur. The information on the area was examined by cyclic voltammetry. Fig. 4 shows the cyclic voltammograms for the catalyst layer in Ar-saturated 0.1 mol dm^{-3} $HClO_4$. The voltammograms for the GNI and GHI layers were almost the same as that for the GWI layer. The sign of the current due to the oxidation reactions was taken as positive and that due to the reduction reactions was taken as negative. The current was generated by charging of the electrochemical double-layer and the redox reaction of quinone-like

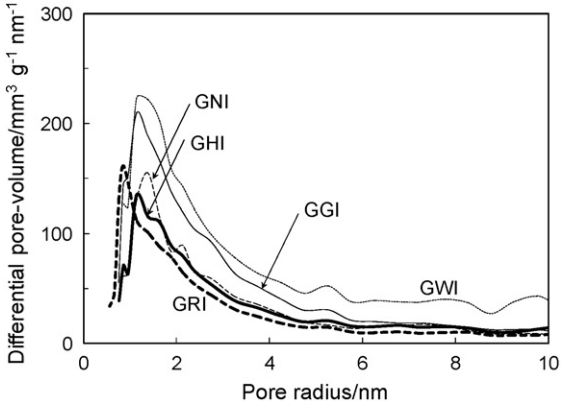

Fig. 3. Pore-size distributions of GGI (thin line), GWI (thin dotted line), GNI (thin dashed line), GHI (thick line), and GRI (thick dashed line).

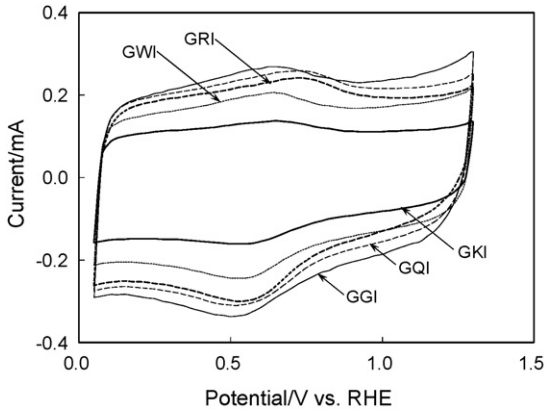

Fig. 4. Cyclic voltammograms for catalyst layers formed using GGI (thin line), GWI (thin dotted line), GQI (thin dashed line), GKI (thick line), and GRI (thick dashed line) in Ar-saturated 0.1 mol dm^{-3} $HClO_4$ at 25 °C. Scan rate: 50 mV s^{-1}.

functional groups (Qn) on the surfaces, which is usually observed for carbon electrodes [54]:

$$Qn + 2H^+ + 2e^- \leftrightarrow QnH_2 \quad (1)$$

In theory, the charging current of the electrochemical double layer is proportional to the electrochemically active surface area. The oxidation and reduction reactions of the quinone-like functional groups were observed as the broad peaks centered at around 0.65–0.7 and 0.5–0.55 V, respectively. Almost all the currents at the layers of the catalysts formed using the nitrogen-rich amino acids were smaller than that at the GGI layer. This behavior was associated with the smaller specific surface area.

3.3. Oxygen reduction

Oxygen reduction currents at the catalyst layers were measured in O_2-sarturated 0.1 mol dm^{-3} $HClO_4$ with the electrodes being rotated at various rotation speeds. Fig. 5 shows the relationships between the electrode potential and the currents at the catalyst layers measured by rotating the electrodes at 2000 rpm. The current shown in Fig. 5 was obtained by subtracting the background current from the measured current. The O_2 reduction current was varied with the kind of amino acids used as the starting materials for the catalysts.

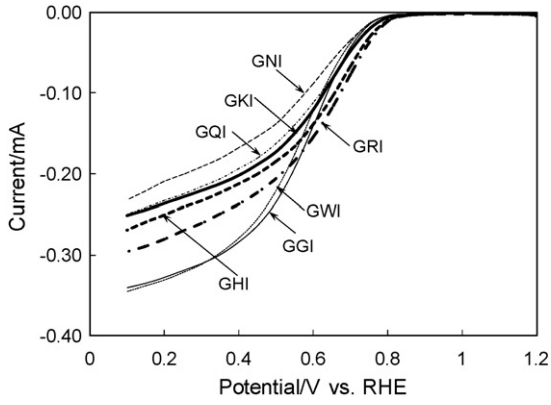

Fig. 5. Relationships between electrode potential and oxygen reduction current of negative scans at catalyst layers formed using GGI (thin line), GWI (thin dotted line), GNI (thin dashed line), GQI (thin chain line), GKI (thick line), GHI (thick dashed line), and GRI (thick chain line) in O_2-saturated 0.1 mol dm^{-3} $HClO_4$ at 25 °C. Scan rate: 10 mV s^{-1}. Electrode rotation speed: 2000 rpm.

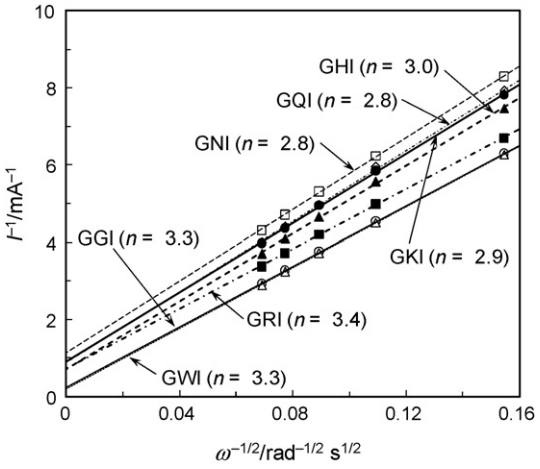

Fig. 6. $-1/I$ vs. $\omega^{-1/2}$ plots for oxygen reduction and number of electrons involved in the reaction per molecule at 0.1 V for catalyst layers formed using GGI (○, thin line), GWI (△, thin dotted line), GNI (□, thin dashed line), GQI (◊, thin chain line), GKI (●, thick line), GHI (▲, thick dashed line), and GRI (■, thick chain line).

The activities of the catalyst layers for O_2 reduction were evaluated using the reduction current free of the influence of mass transfer in the solution, I_K, determined by the equation shown below [49]:

$$-\frac{1}{I} = -\frac{1}{I_K} + \frac{1}{0.620nFAD^{2/3}c\nu^{-1/6}\omega^{1/2}} \quad (2)$$

where I is the reduction current after subtracting the background current, n is the number of electrons involved in the O_2 reduction per molecule, F is the Faraday constant, A is the geometric area of the GC electrode, D is the diffusion coefficient of O_2 in the solution, c is the concentration of O_2 in the solution, ν is the kinematic viscosity of the solution, and ω is the angular frequency of the rotation. Fig. 6 shows $-1/I$ vs. $\omega^{-1/2}$ plots for the O_2 reduction at 0.1 V and n that were calculated using the slope of the plot and the following values [55–57]: F, 96,485 C mol^{-1}; A, 0.0707 cm^2; D, 1.9×10^{-5} cm^2 s^{-1}; c, 1.18×10^{-6} mol cm^{-3}; ν, 9.87×10^{-3} cm^2 s^{-1}. The relationships between the electrode potential and $\log(-I_K/A)$ (Tafel plots) are shown in Fig. 7. The I_K up to 0.8 V was displayed because I_K above 0.8 V contained large error due to the small I above 0.8 V as shown in Fig. 5.

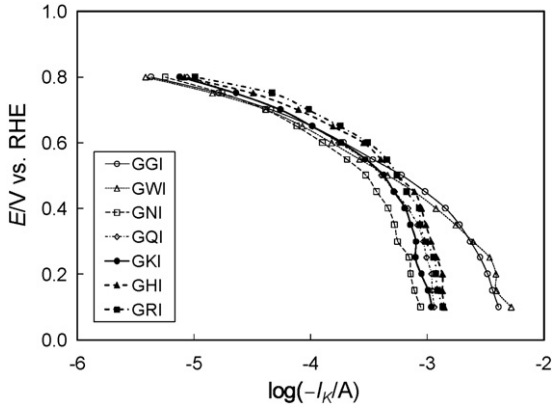

Fig. 7. Relationships between electrode potential and $\log(-I_K/A)$ for catalyst layers formed using GGI (○, thin line), GWI (△, thin dotted line), GNI (□, thin dashed line), GQI (◊, thin chain line), GKI (●, thick line), GHI (▲, thick dashed line), and GRI (■, thick chain line).

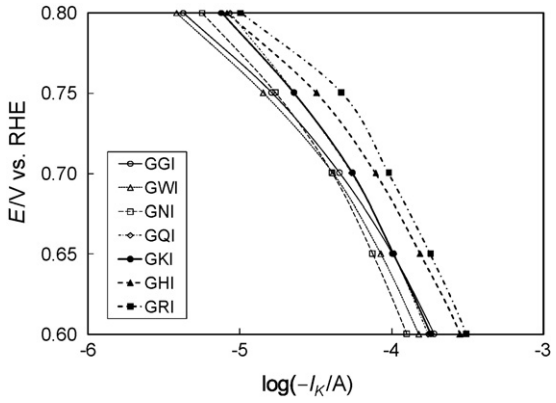

Fig. 8. Expanded view of the Tafel plots shown in Fig. 7 in the range from 0.6 to 0.8 V.

3.4. Efficiency for active site generation

The current in the high potential region in the Tafel slope shown in Fig. 7 was closely associated with the intrinsic activity of the catalyst since the influence of the mass transfer in the catalyst layer was small. The expanded view of the plot in the range from 0.6 to 0.8 V is shown in Fig. 8. The $-I_K$ in the high potential region was dependent on the number of nitrogen atoms in the amino acid used as the starting material. The $-I_K$ above 0.65 V at the GQI and GKI layers and the $-I_K$ above 0.75 V at the GNI layer were higher than that at the GGI layer; however, the $-I_K$ at the GWI was lower, indicating that the enhancement effect for oxygen reduction using the amino acid containing 2 nitrogen atoms in the molecule was small. In contrast, the $-I_K$ at the GHI layer was higher than those at the above 5 catalyst layers except only near 0.8 V and the $-I_K$ at the GRI layer further increased. This result indicated that the activity for oxygen reduction increased with an increase in the number of nitrogen atom contained in the amino acid molecule.

Fig. 9 shows the XPS of Fe 2p in GGI and GRI. Both peak positions of the Fe $2p_{3/2}$ binding energy situated 711.0 eV, showing that the oxidation states were III based on the peak position of the Fe $2p_{3/2}$ binding energy for Fe(III), 710.8–711.8 eV [58,59]. It has been reported by Widelöv et al. that a negative peak shift of the Fe $2p_{3/2}$ occurred along with the activity increase for the O_2 reduction at the catalyst formed by pyrolyzing Fe(III) tetra(*p*-chlorophenyl)porphyrin chloride adsorbed on carbon black [18].The negative shift could be attributed to the increase in Fe(II) based on the peak position of the Fe $2p_{3/2}$ binding energy for Fe(II), 707.1–708.7 eV [58,59]. The activity increase with an increase in

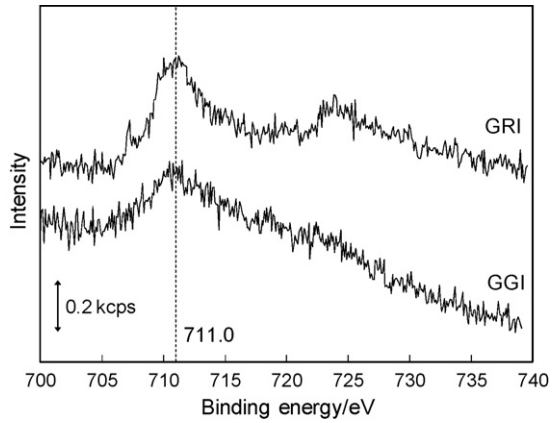

Fig. 9. X-ray photoelectron spectra of Fe 2p in GGI and GRI. Each spectrum was arbitrarily shifted in the *y*-axis direction for easier comparison.

Table 2
Ratios of elements on the surface of GGI, GQI, and GRI (at.%)

	GGI	GQI	GRI
C	97.21	95.76	94.69
N	0.54	0.64	0.99
O	2.15	3.51	4.15
Fe	0.10	0.08	0.17

The ratios of the elements on the surface of the carbon materials were calculated assuming that those of the elements other than C, N, O, and Fe were negligible since the raw materials were nominally composed of these elements.

Fe(II) could be explained by applying the O_2 reduction mechanism proposed by Bouwkamp-Wijnoltz et al. for the pyrolyzed Fe porphyrin adsorbed on carbon, in which Fe(II) on the catalyst surface is required as an O_2 bonding site during the first step of the multistep reaction [22]. Therefore, the results in this study excluded the possibility of the activity enhancement by the change of the Fe oxidation state. The pore development in the catalyst could be another factor for the activity enhancement [60]; however, the pore development in GRI was lower than in GGI, also excluding the possibility of the activity enhancement by this factor.

The parameter most related to the activity enhancement was the Fe content in the catalyst. The $-I_K$ tended to increase with an increase in the Fe content, except for the GQI layer. The disagreement between the highest Fe content in GQI and the $-I_K$ at the GQI layer was attributed to the low ratio of Fe atoms on the surface of the catalyst (Table 2). In GQI, the Fe might be included in the carbon matrix of the catalyst and would not be exposed to the surface. In contrast, the higher ratios of Fe and nitrogen atoms on the surface were observed for the GRI. This result indicated that the Fe–N_x active site efficiently generated on the surface by the application of the nitrogen-rich amino acids to the catalyst formation and that the efficiency was increased by an increase in the number of nitrogen atoms in the amino acid.

The efficient generation was also indicated by the results of the EXAFS measurements at the Fe K-edge for the catalyst. Fig. 10 shows the Fe K-edge RDFs for the Fe foil, α-Fe_2O_3, γ-Fe_2O_3, hematin, GGI, G3GI, G4GI, and GRI. In the spectrum for hematin, the first peak at around 1.7 Å was attributed to four nitrogen atoms coordinating to the Fe(III) center. The shoulder at around 1.2 Å was attributed to OH^- coordinating perpendicular to the macrocyclic plane to the Fe center. The second peak was attributed to the C atoms, which were bound to the nitrogen atom in the pyrolic ring and the bridging C connecting the pyrolic rings. Comparing the spectrum for GGI with that for hematin, the peak at 1.5 Å and the shoulder at around 3 Å observed in the spectrum for GGI were attributed to the Fe–N_x active site. Although it is recognized that the identification of the nearest neighbor atom only from the EXAFS result is difficult, it might be reasonable to assume the presence of the Fe–N_x moiety in the catalysts formed using the amino acids as the N sources on the basis of the results of the Mössbauer spectrum of GGI shown in reference 47, which was similar to the carbonized catalase containing the Fe–N_x moiety. The first peak position negatively shifted, suggesting that the distance between Fe and nitrogen was shorter than that in hematin. The largest peak at 2.2 Å in the spectrum was attributed to the Fe(0) included in the carbon matrix of GGI, comparing the spectrum to that for the Fe foil. The spectra for G3GI and G4GI showed that the peak attributed to the Fe(0) decreased with an increase in the glycine content in the starting mixture and the peak finally disappeared in the spectrum for GRI, indicating that the Fe–N_x active site was generated efficiently by the increase in the nitrogen content in the starting mixture without generating the Fe(0), although the peak at 2.8 Å was partly attributed to the α-Fe_2O_3 and γ-Fe_2O_3 included in the carbon matrix according to the XRD result.

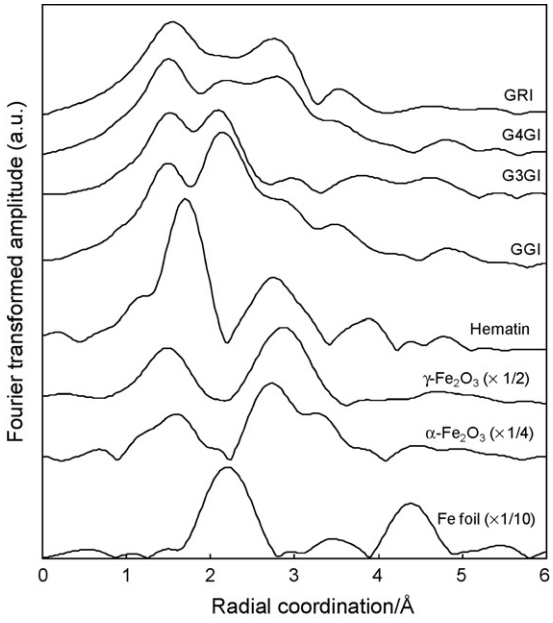

Fig. 10. Pseudo-radial distribution functions calculated by Fourier transformation of extended X-ray adsorption fine spectra at the Fe K-edge for Fe foil, α-Fe_2O_3, γ-Fe_2O_3, hematin, GGI, G3GI, G4GI, and GRI.

In this study, we focused on the effect of the number of nitrogen atoms in the amino acids on the active site generation and fuel cell tests using the catalysts formed in this study were omitted. Studies are being carried out in order to obtain the information on the mechanism of the active site generation using other kind of nitrogen sources. Further studies are also necessary for investigating the degradation behavior of the active site, because it has been recognized that the degradation rate of the Fe–N_x active site is faster than the conventional Pt-based catalyst and the improvement of its durability is an important subject as well as the improvement of the activity.

3.5. Number of electrons involved in O_2 reduction per molecule

An increase in n was also observed with the number of nitrogen atoms in the amino acids used for the catalyst formation except for the GGI and GWI layer, in which n was as high as that for the GRI layer in spite of the small number of nitrogen atoms in the amino acid used for the catalyst formation. A two-electron reduction generates the intermediate H_2O_2 (Eq. (3)). An increase in n occurs with further reduction (Eq. (4)), the decomposition of H_2O_2 (Eq. (5)), or an increase in the proportion of the four-electron reduction to H_2O (Eq. (6)) [61].

$$O_2 + 2H^+ + 2e^- \rightarrow H_2O_2 \quad (3)$$

$$H_2O_2 + 2H^+ + 2e^- \rightarrow 2H_2O \quad (4)$$

$$2H_2O_2 \rightarrow 2H_2O + O_2 \quad (5)$$

$$O_2 + 4H^+ + 4e^- \rightarrow 2H_2O \quad (6)$$

The n increase is caused by the increase in the active site and the development of the micropores in the catalyst, because the latter raised the possibility that H_2O_2 molecules generated inside the catalyst layer were further reduced or decomposed during their transfer to the outside of the layer, which resulted in the n increase. Except for GGI and GWI, the increase in n was attributed to the increase in the active site in the catalyst due to the similar extent of the pore development for the five catalysts. The high n for the

GGI and GWI layer might be due to the developed pore structure in the catalyst particles. The developed pore structure was also the reason for the higher $-I_K$ in the low potential region at the GGI and GWI layer than the other catalyst layers, due to the feasibility of the mass transfer inside the catalyst particles.

4. Conclusions

The noble-metal-free PEFC cathode catalysts were formed as carbon materials with the Fe–N_x moiety embedded on the surface as the active site for oxygen reduction using glucose, iron lactate, and amino acids which contain more than one nitrogen atom in each molecule. Such nitrogen-rich amino acids were chosen from the 20 amino acids that constitute proteins: tryptophan, asparagine, glutamine, and lysine (2 nitrogen); histidine (3 nitrogen); arginine (4 nitrogen), and were used in this study. The oxygen reduction current at the catalyst layer formed from the carbon material was dependent on the molecular structure of the amino acid used as the starting material. The activity of the catalyst increased with an increase in the number of nitrogen atoms in the amino acid molecule and this activity increase was attributed to the improved efficiency of the Fe–N_x active site generation, which was verified by the Fe contents in the catalysts, the XPS results, and the results of the EXAFS measurements. These results thus provided fundamental information on the improvement in the activity of the carbon-based noble-metal-free catalysts for their practical utilization.

Acknowledgments

We thank Mr. H. Kawano for his help with the ICP-AES measurements, and Dr. T. Shinagawa for providing the EXAFS data of Fe_2O_3. The XAFS measurements were performed with the approval of the SPring8 (Proposal nos. 2003A0863-RI-np and 2007A1470). We thank Dr. Y. Uchimoto, J. Okamura and the SPring8 members for their kind support of the measurements and the analysis. This study was partly supported by a Grant-in-Aid for Scientific Research (project no. 18750183) given to J.M. from the Ministry of Education, Culture, Sports, Science and Technology, Japan, for which the authors are grateful.

References

[1] M.Z. Jacobson, W.G. Colella, D.M. Golden, Science 308 (2005) 1901–1905.
[2] W. Vielstich, A. Lamm, H.A. Gasteiger (Eds.), Handbook of Fuel Cells, John Wiley & Sons, Chichester, 2003.
[3] B.C.H. Steele, A. Heinzel, Nature 414 (2001) 345–352.
[4] P. Costamagna, S. Srinivasan, J. Power Sources 102 (2001) 242–252.
[5] S. Gottesfeld, T.A. Zawodzinski, in: R.C. Alkire, H. Gerischer, D.M. Kolb, C.W. Tobias (Eds.), Advances in Electrochemical Science and Engineering, vol. 5, Wiley–VCH, Weinheim, 1997, p. 195.
[6] H.A. Gasteiger, J.E. Panels, S.G. Yan, J. Power Sources 127 (2004) 162–171.
[7] J.-P. Dodelet, in: J.H. Zagal, F. Bedioui, J.-P. Dodelet (Eds.), N_4–Macrocyclic Metal Complexes, Springer, New York, 2006, p. 83.
[8] R. Bashyam, P. Zelenay, Nature 443 (2006) 63–66.
[9] Y. Liu, A. Ishihara, S. Mitsushima, N. Kamiya, K.-I. Ota, J. Electrochem. Soc. 154 (2007) B664–B669.
[10] P.H. Matter, E. Wang, M. Arias, E.J. Biddinger, U.S. Ozkan, J. Mol. Catal. A 264 (2007) 73–81.
[11] J.-I. Ozaki, N. Kimura, T. Anahara, A. Oya, Carbon 45 (2007) 1847–1853.
[12] K. Kinoshita, Electrochemical Oxygen Technology, John Wiley & Sons, New York, 1992.
[13] O. Ikeda, H. Fukuda, H. Tamura, J. Chem. Soc., Faraday Trans. 82 (1986) 1561–1573.
[14] R. Holze, I. Vogel, W. Vielstich, J. Electroanal. Chem. 210 (1986) 277–286.
[15] S. Dong, R. Jiang, Ber. Bunsenges. Phys. Chem. 91 (1987) 479–484.
[16] T. Sawaguchi, T. Itabashi, T. Matsue, I. Uchida, J. Electroanal. Chem. 279 (1990) 219–230.
[17] A. Widelöv, R. Lasson, Electrochim. Acta 37 (1992) 187–197.
[18] A. Widelöv, Electrochim. Acta 38 (1993) 2493–2502.
[19] B. Bittins-Cattaneo, S. Wasmus, B. Lopez-Mishima, V. Vielstiech, J. Appl. Electrochem. 23 (1993) 625–630.
[20] G. Faubert, G. Lalande, R. Côté, D. Guay, J.P. Dodelet, L.T. Weng, P. Bertrand, G. Dénès, Electrochim. Acta 41 (1996) 1689–1701.
[21] G. Faubert, R. Côté, D. Guay, J.P. Dodelet, G. Dénès, P. Bertrand, Electrochim. Acta 43 (1998) 341–353.
[22] A.L. Bouwkamp-Wijnoltz, W. Visscher, J.A.R. van Veen, Electrochim. Acta 43 (1998) 3141–3152.
[23] S.L. Gojković, S. Gupta, R.F. Savinell, J. Electroanal. Chem. 462 (1999) 63–72.
[24] R. Jiang, D. Chu, J. Electrochem. Soc. 147 (2000) 4605–4609.
[25] M. Lefèvre, J.P. Dodelet, P. Bertrand, J. Phys. Chem. B 104 (2000) 11238–11247.
[26] M. Lefèvre, J.P. Dodelet, P. Bertrand, J. Phys. Chem. B 106 (2002) 8705–8713.
[27] A.L. Boukamp-Wijnoltz, W. Visscher, J.A.R. van Veen, E. Boellaard, A.M. van der Kraan, S.C. Tang, J. Phys. Chem. B 106 (2002) 12993–13001.
[28] M. Lefèvre, J.P. Dodelet, Electrochim. Acta 48 (2003) 2749–2760.
[29] H. Schulenburg, S. Stankov, V. Schu1nemann, J. Radnik, I. Dorbandt, S. Fiechter, P. Bogdanoff, H. Tributsch, J. Phys. Chem. B 107 (2003) 9034–9041.
[30] J.A.R. van Veen, H.A. Colijn, J.F. van Baar, Electrochim. Acta 33 (1988) 801–804.
[31] G. Lalande, G. Faubert, R. Côté, D. Guay, J.P. Dodelet, L.T. Weng, P. Bertrand, J. Power Sources 61 (1996) 227–237.
[32] M. Bron, J. Radnik, M. Fieber-Erdmann, P. Bogdanoff, S. Fiechter, J. Electroanal. Chem. 535 (2002) 113–119.
[33] K. Sawai, N. Suzuki, J. Electrochem. Soc. 151 (2004) A2132–A2137.
[34] S. Gupta, D. Tryk, I. Bae, W. Aldred, E. Yeager, J. Appl. Electrochem. 19 (1989) 19–27.
[35] C. Fabjan, G. Frithum, H. Hartl, Ber. Bunsenges. Phys. Chem. 94 (1990) 937–941.
[36] D. Ohms, S. Herzog, R. Franke, V. Neumann, K. Wiesener, S. Gamburcev, A. Kaisheva, I. Iliev, J. Power Sources 38 (1992) 327–334.
[37] R. Côté, G. Lalande, D. Guay, J.P. Dodelet, G. Dénès, J. Electrochem. Soc. 145 (1998) 2411–2418.
[38] S. Ye, A.K. Vijh, Electrochem. Commun. 5 (2003) 272–275.
[39] J. Fournier, G. Lalande, R. Côté, D. Guay, J.P. Dodelet, J. Electrochem. Soc. 144 (1997) 218–226.
[40] F. Jaouen, J.-P. Dodelet, J. Phys. Chem. C 111 (2007) 5963–5970.
[41] H. Wang, R. Côté, G. Faubert, D. Guay, J.P. Dodelet, J. Phys. Chem. B 103 (1999) 2042–2049.
[42] J. Maruyama, I. Abe, Chem. Mater. 17 (2005) 4660–4667.
[43] J. Maruyama, I. Abe, Chem. Mater. 18 (2006) 1303–1311.
[44] J. Maruyama, J. Okamura, K. Miyazaki, I. Abe, J. Phys. Chem. C 111 (2007) 6597–6600.
[45] J.M. Jones, Q. Zhu, K.M. Thomas, Carbon 37 (1999) 1123–1131.
[46] A.J. Herod, T.C. Gibb, A.A. Herod, B. Xu, S. Zhang, R. Kandiyoti, Fuel 75 (1996) 437–442.
[47] J. Maruyama, I. Abe, J. Electrochem. Soc. 154 (2007) B297–B304.
[48] J. Maruyama, I. Abe, Chem. Commun. (2007) 2879–2881.
[49] J. Maruyama, I. Abe, Electrochim. Acta 48 (2003) 1443–1450.
[50] F. Gloaguen, F. Andolfatto, R. Durand, P. Ozil, J. Appl. Electrochem. 24 (1994) 863–869.
[51] S.Lj. Gojković, S.K. Zečević, R.F. Savinell, J. Electrochem. Soc. 145 (1998) 3713–3720.
[52] D. Chu, D. Tryk, D. Gervasio, E.B. Yeager, J. Electroanal. Chem. 272 (1989) 277–284.
[53] M. Razaq, A. Razaq, E. Yeager, D.D. DesMarteau, S. Singh, J. Electrochem. Soc. 136 (1989) 385–390.
[54] J. Maruyama, I. Abe, Electrochim. Acta 46 (2001) 3381–3386.
[55] J. Maruyama, I. Abe, J. Electroanal. Chem. 545 (2003) 109–115.
[56] S.K. Zečević, J.S. Wainright, M.H. Litt, S.Lj. Gojković, R.F. Savinell, J. Electrochem. Soc. 144 (1997) 2973–2982.
[57] R.M.Q. Mello, E.A. Ticianelli, Electrochim. Acta 42 (1997) 1031–1039.
[58] L.Y. Johansson, R. Larsson, Chem. Phys. Lett. 24 (1974) 508–513.
[59] T. Choudhury, S.O. Saied, J.L. Sullivan, A.M. Abbot, J. Phys. D: Appl. Phys. 22 (1989) 1185–1195.
[60] J. Maruyama, J. Okamura, K. Miyazaki, I. Abe, J. Phys. Chem. C 112 (2008) 2784–2790.
[61] J. Maruyama, M. Inaba, T. Morita, Z. Ogumi, J. Electroanal. Chem. 504 (2001) 208–216.